Modelling Pullout Behavior of Reinforcement Material

Ching-Chuan Huang

Professor Emeritus
Department of Civil Engineering,
National Cheng Kung University, Tainan, Taiwan
Email: samhcc@mail.ncku.edu.tw
2025/11/28

INTRODUCTION

In displacement-based analyses using the Finite Failure Displacement Method (FFDM), the mobilized pullout forces of reinforcement are governed by shear displacements along the potential failure surface. Past investigations into the tensile stress–pullout displacement behavior of reinforcing materials subjected to pullout have demonstrated that these relationships can be effectively represented using hyperbolic curves.

To construct a hyperbolic curve-based reinforcement pullout model, a series of well-instrumented pullout tests on polymer and non-polymer reinforcements were analyzed using curve-fitting techniques. Preliminary studies by Huang (2013) and Huang et al. (2017) explored the application of hyperbolic modeling in reduced-scale pullout tests involving geosynthetic materials.

In this report, the hyperbolic curve-based pullout model is further developed to accommodate a broader range of materials currently employed as reinforcements. Additionally, correlations between soil types and the governing parameters of the hyperbolic pullout curves are identified.

13.1 BOND COEFFICIENT

Experimental studies on soil-reinforcement interactions using pullout boxes (**Table 13.1.1**) provide information in terms of pullout interaction coefficient, f_b defined by:

$$f_b = \frac{\tau_{max}}{\tau_f} \qquad (13-1-1)$$

τ_{max}: peak value of shear stress mobilized at peak pullout force.

τ_f: shear strength of soils

Values of f_b obtained from the pull-out tests presented in **Fig. 13.1.1** reveal the following observations:

(1) A consistent decreasing trend in f_b with increasing effective normal stress (σ_n') is observed across all tested materials - except for the geogrid/clayey silt interface, which displays pressure-independent f_b values.

(2) The f_b values for the smooth steel/sand interface are comparable to those observed for geogrid/sand and geotextile/sand interfaces.

(3) Ribbed materials, such as ribbed geo-strips and ribbed steel strips, exhibit f_b values that are clearly distinguishable from those associated with smooth-faced materials.

(4) The ribbed geo-strip/sand interface shows relatively high variability in f_b, as indicated by the upper-limit curve shown for this interface in **Fig. 13.1.1**.

Table 13.1.1 Summary of pullout test set-up

Reference	Soil type (USCS)	Pullout material	L_f* (m)	c ** (kPa)	φ** (°)	σ'_n (kPa)
Sugimoto & Alagiyawanna (2003)	Silica sand (SP)	Integrated geogrid	0.5 (SS-1) 0.54 (SR-55)	0	29.9	5- 93
Sieira et al. (2009)	Sandy silt (SM), silty clay (MC)	Woven geogrid	1.0	15-30	21-37	5- 25
Moraci et al. (2014)	Silica sand (SP)	Geogrid	1.15		48***	10- 100
Tajabadipour & Lajevardi (2021)	Silica sand (SP)	Geosynthetic, Steel, Ribbed steel strips	0.85	0	38	25- 75
Ismail et al. (2021)	Silica sand (SP)	Biaxial geogrid, Wonen geotextile	0.70	0	46.8-52.6	100-200
Park & Hong (2021)	Well-graded sand (SW)	Geosynthetic strip	1.25	8.7	35.5	50- 150
Vieira & Pereira (2022)	Re-cycled construction materials (SM)	Woven geogrid, Woven geotextile	0.75	16.3	37.6	10- 25

* Full embedment length of pullout specimen

** Cohesion intercept and internal friction angle of soils

*** $\varphi_0 = 48^\circ$, $\Delta\varphi = 6^\circ$; $\varphi = \varphi_0 - \Delta\varphi \bullet \log(\sigma'_n / P_a)$; P_a: atmospheric pressure (= 101.3 kPa)

Table 13.1.2 Summary of pullout test results for geosynthetic materials

Reference	Geogrid ID / USCS	$T_{tiebreak}$ in kN/m	μ [2] *in degree*	μ / φ
Sugimoto &	SS-1/SP	15.3[1]	9.2- 16.2	0.3- 0.54
Alagiyawanna (2003)	SR-55/SP	54.0	17.5- 20.0	0.58- 0.67
Sieira et al. (2009)	MG/SM	97.0	35.9- 37.3	0.91- 1.01
	MG/MC	97.0	11.2- 14.1	0.53- 0.67
Moraci et al. (2014)	GG3/SP	118.0	35.3- 52.4	0.73- 1.09
Tajabadipour &	GS[4]/SP	50.0 /0.09m	21.8- 42.5	0.57- 1.12
Lajevardi (2021)	CGS[4]/SP	50.0/ 0.09m	36.5- 55.2	0.96-1.45
Ismail et al. (2021)	WGT/SP_coarse	109.0	26.5- 31.1	0.50- 0.58
	WGT/SP_fine	109.0	21.4- 34.1	0.46- 0.73
Park & Hong (2021)	GS70W[5]/SW	25.0/ 0.07m	49.7- 60.8	1.40- 1.71
Vieira & Pereira	GGR/SM[3]	80.0	37.4- 37.9	0.99- 1.00
(2022)	GCR/SM[3]	75.0	32.0- 34.2	0.85- 0.91

(1) Estimated tensile strength at tensile strain > 15%.

(2) $\mu = tan^{-1}(f_b * \tau_f)$; *$f_b$: pullout interaction coefficient;* $\tau_f = \sigma'_v \bullet tan\ \varphi$

(3) Silty sand under *Optimum Moisture Content (OMC)* conditions

(4) Geosynthetic strip with a width of 0.09m

(5) GS: Geosynthetic strip; CGS: Geosynthetic strip with ribs

(6) GS70W: 0.07m-wide geosynthetic strip with ribs

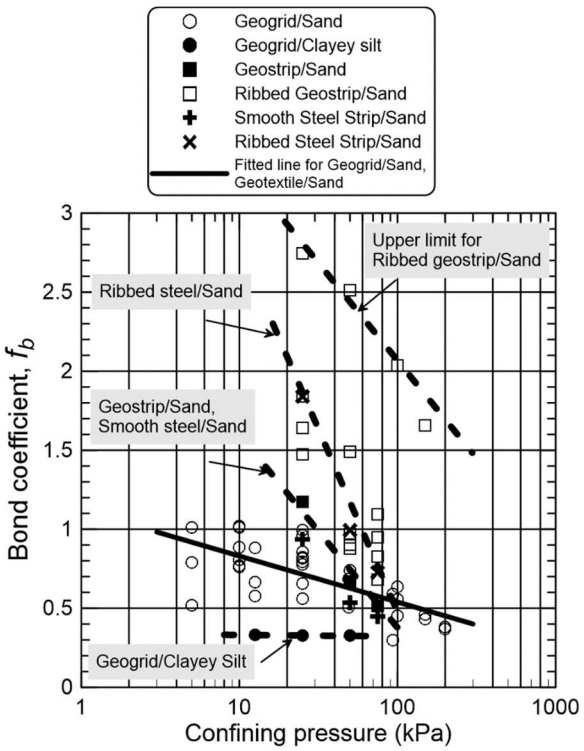

Fig. 13.1.1 Pullout interaction coefficients obtained for various materials

An important consideration when applying the previously discussed f_b values is the appropriate length of reinforcement within the potential pullout zone—specifically, whether to use the full embedded length (L_f) or the so-called "effective length" (L_e). The latter has been identified and proposed in recent studies (Cardile et al., 2016).

As shown in **Table 13.1.1**, only a limited number of pullout tests with $L_f > 1.0$ m were conducted using local strain or displacement sensors. Consequently, an assumption of $L_e \leq 1.0$ m is adopted here for deriving the bond coefficients illustrated in **Fig. 13.1.1**.

Further support for the use of $L_e \leq 1.0$ m is provided by findings from Cardile et al. (2016) and Ferreira et al. (2020), which indicate that, under peak pullout conditions, local axial stresses (or strains) beyond 1.0 m from the pullout end become negligibly small.

13.2 HYPERBOLIC PULLOUT FORCE-DISPLACEMENT RELATIONSHIPS

The hyperbolic pullout force vs. displacement curve can be expressed as:

$$T_p = \frac{\delta}{a + b \cdot \delta} \qquad (13-2-1)$$

$$a = \frac{1}{k_i} \qquad (13-2-2)$$

$$b = \frac{1}{T_{spt}} = \frac{R_t}{T_f} \qquad (13-2-3)$$

δ: pullout displacement

k_i: initial pullout stiffness

R_t: asymptote factor (ratio between failure strength and asymptote strength)

T_{spt}: asymptote strength at infinite displacement

T_f: failure strength determined by the smallest among the tiebreak, the pullout from front-side, and the pullout from back-side of the slip surface.

$$T_f = Min.of\left\{T_{pullout\_front}, T_{pullout\_back}, T_{tiebreak}\right\} \qquad (13-2-4)$$

$$T_{pullout\_front} = f_b \cdot \sigma_n' \cdot \tan\varphi \cdot L_{e\_front} \qquad (13-2-5)$$

$$T_{pullout\_back} = f_b \cdot \sigma_n' \cdot \tan\varphi \cdot L_{e\_back} \qquad (13-2-6)$$

σ_n': Effective normal stress

L_{e_front}, L_{e_back}:Effective pullout length of reinforcement at front-side and back-side, respectively, of the slip surface. ($\leqq$1.0 m is suggested)

$T_{tiebreak}$: tie-break strength of reinforcement

13.3 STRESS DEPENDENCY OF INITIAL PULLOUT STIFFNESS

The initial pullout stiffness (k_i) can be expressed as a power function of effective normal stress (σ_n') on the failure surface:

$$k_i = K_t \cdot G_t \left(\frac{\sigma'_n}{P_a}\right)^{n_t} \qquad (13-3-1)$$

K_t: initial pullout stiffness number (a non-dimensional material constant)

P_a: atmospheric pressure (= 101.3 kPa)

G: reference pullout stiffness (= 101.3 kN/m/m)

n_t: exponent of stress dependency

Based on a series of curve-fitting analyses of pullout resistance versus pullout displacement data reported in the studies listed in **Table 13.1.1**, the hyperbolic curve parameters—K_t, n_t, and R_t—are summarized in Figs. 13.3.1 (and **13.3.2**), **13.3.3**, and **13.3.4**, respectively. Each figure presents a median line along with 95% confidence intervals.

To categorize soil types, the Unified Soil Classification System (USCS) designations are used: Type 1: SW, Type 2: SP, Type 3: SM, and Type 4: MC. These classifications are preferred over friction angles (φ) because one of the tested soils is cohesive, exhibiting a non-zero cohesion intercept—thus, friction angle alone does not fully characterize soil strength.

Figure 13.3.1 illustrates the relationship between K_t and soil type as observed in the pullout tests. A general trend of decreasing K_t values is evident with diminishing soil strength or particle size.

Figure 13.3.2 presents an alternative representation of the K_t - soil type relationship, where the ordinate is defined as the normalized parameter ($Kt \cdot G$ / $J_{2\%}$), with $J_{2\%}$ representing the in-air tensile stiffness of the pullout material. Compared to **Fig. 13.3.1**, the data in **Fig. 13.3.2** exhibit reduced scatter.

Figure 13.3.3 shows the relationship between the stress-level dependency exponent (n_t) and soil type. A declining trend in n_t is observed with reduced soil strength or finer particle size.

Figure 13.3.4 displays the asymptote factor (R_t) plotted against soil type. The observed trend is consistent with those shown in **Figs. 13.3.1** through **13.3.3**, reflecting similar soil-dependent behavior across parameters.

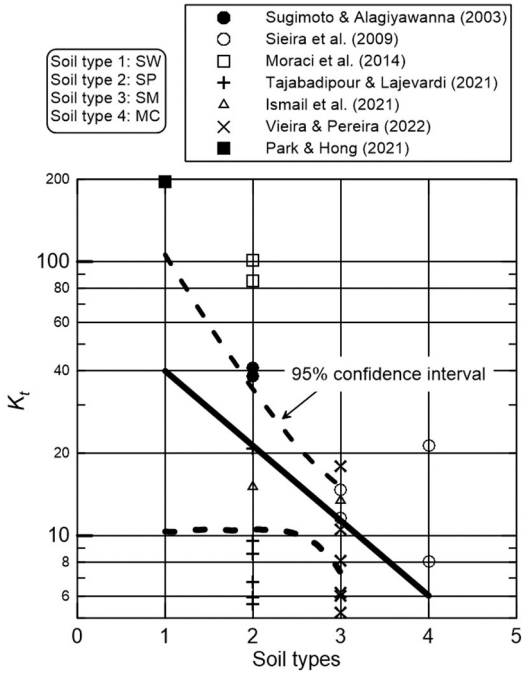

Figure 3.3.1 Initial pullout stiffness number K vs. Soil type relationship

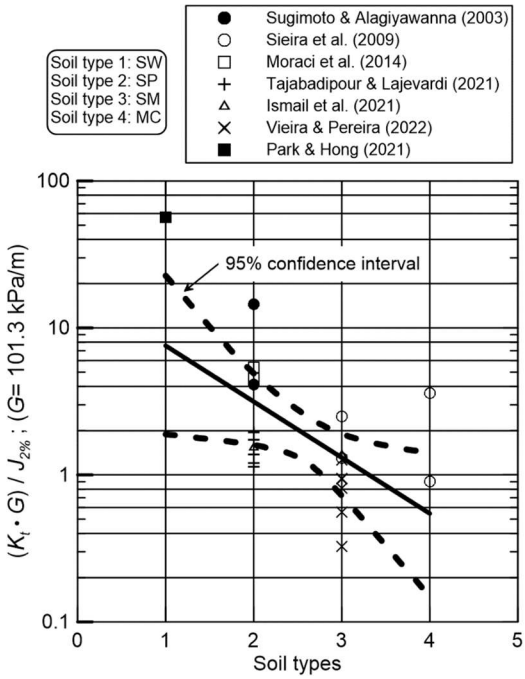

Figure 13.3.2 Normalized initial pullout stiffness number K_t vs. Soil type relationship.

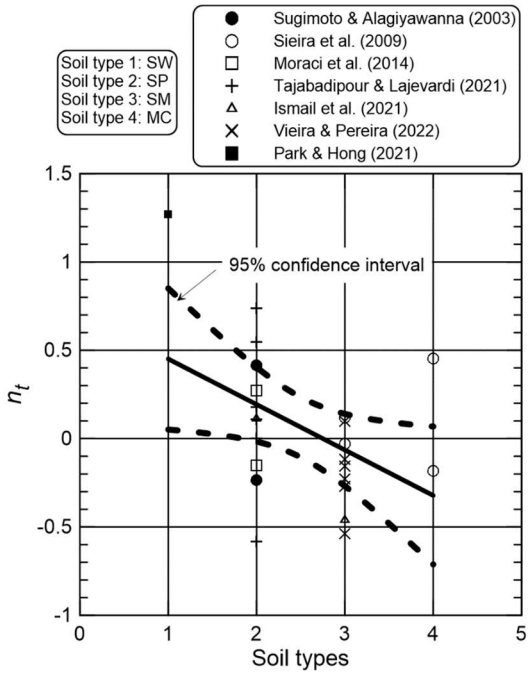

Figure 13.3.3 Pressure dependency exponent (n_t) vs. Soil type relationships

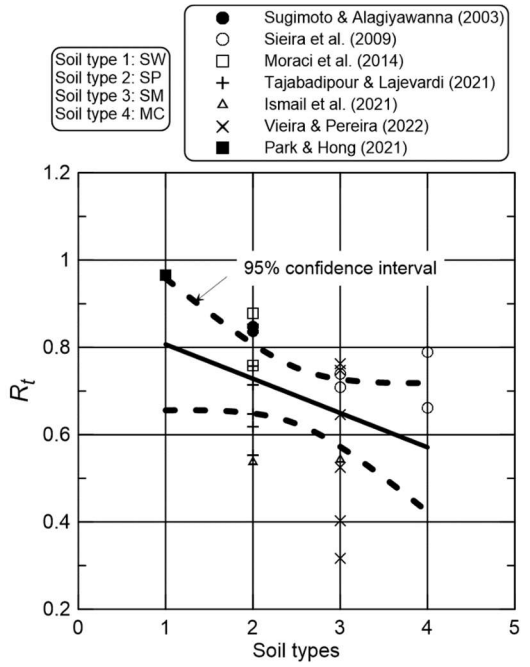

Figure 13.3.4 Asymptote factor (R_t) vs. Soil type relationships

13.4 VERIFICATION OF CURVE FITTED PULLOUT PARAMETERS

To validate the previously described hyperbolic pullout model, parameters extracted from the fitted median lines in Figs. 13.3.1 through **13.3.4** - summarized in Table 13.4.1 - are used to simulate pullout force-displacement curves. Comparisons between experimental and simulated curves for three test series reported by Sieira et al. (2009), Moraci (2014), and Vieira and Pereira (2022) are presented in **Figs. 13.4.4** through **13.4.8**. The simulation results demonstrate generally good agreement with experimental data.

Table 13.4.1 Summary of median line value of hyperbolic pullout parameters

Soil type	K_t	$(K_t \cdot G)/J_{2\%}$	n_t	R_t
Type 1 (SW)	40	7.8	0.45	0.8
Type 2 (SP)	20	3.2	0.2	0.72
Type 3 (SM)	12	1.3	-0.1	0.67
Type 4 (MC)	6	0.5	-0.3	0.58

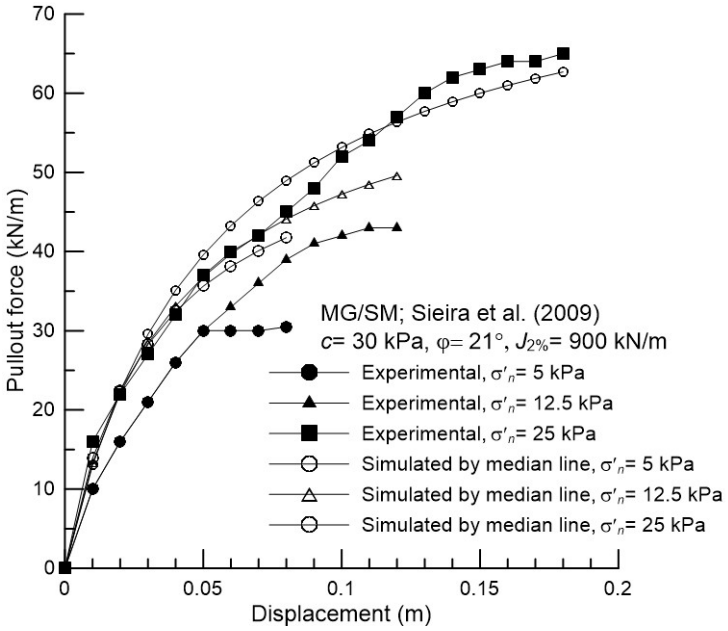

Figure 13.4.4 Comparisons of experimental and simulated pullout force-displacement curves for geogrid/silty sand (MG/SM) reported by Sieira et al. (2009)

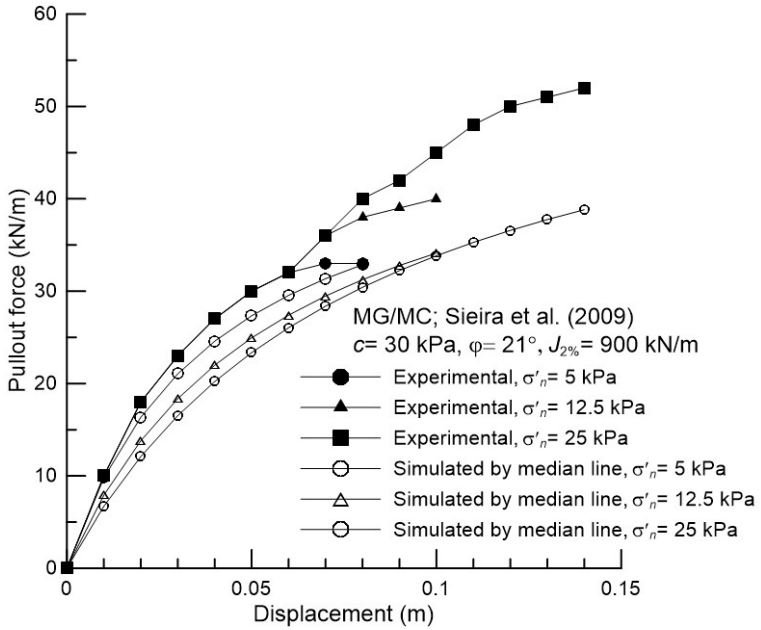

Figure 13.4.5 Comparisons of experimental and simulated pullout force-displacement curves for geogrid/clayey silt (MG/MC) reported by Sieira et al. (2009)

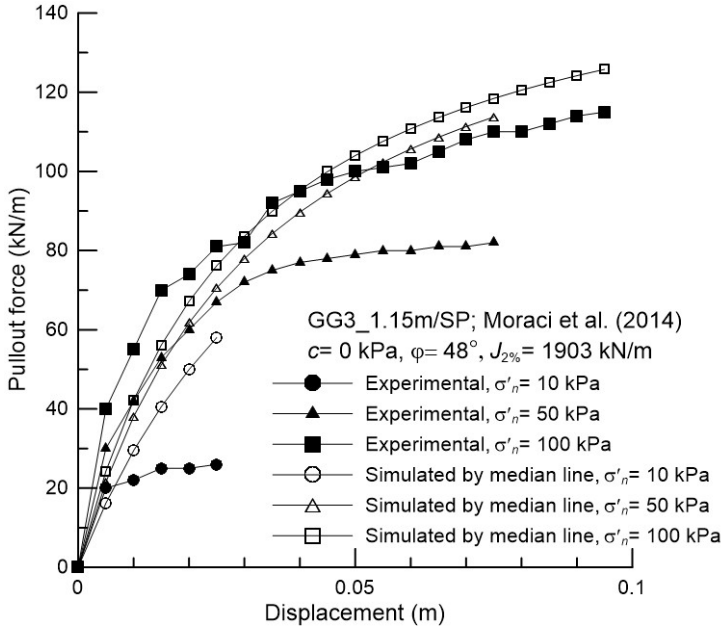

Figure 13.4.6 Comparisons of experimental and simulated pullout force-displacement curves for geogrid/clayey silt (GG3_1.15m/MC) reported by Moraci et al. (2014).

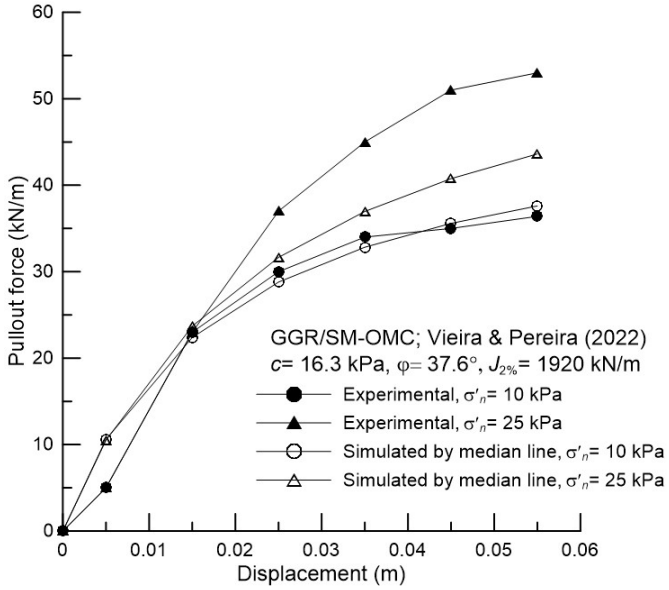

Figure 13.4.7 Comparisons of experimental and simulated pullout force-displacement curves for geogrid/silty sand under optimum water content (GGR/SM-OMC) reported by Vieira and Pereira (2022)

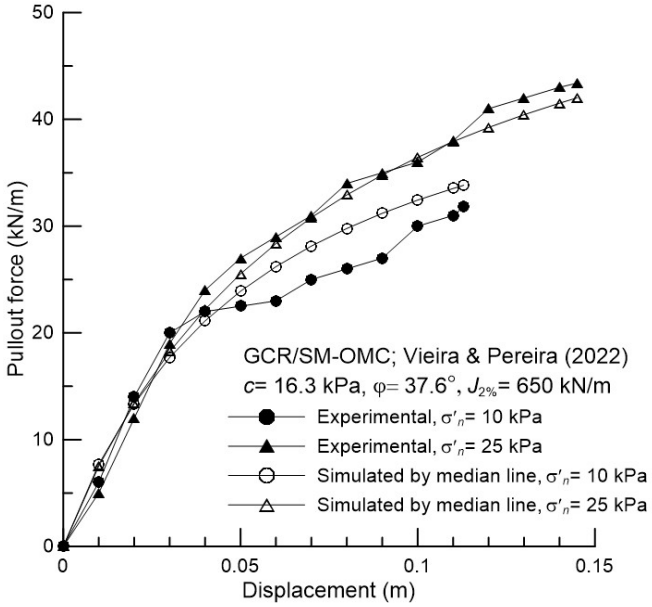

Figure 13.4.8 Comparisons of experimental and simulated pullout force-displacement curves for geogrid/silty sand under optimum water content (GCR/SM-OMC) reported by Vieira and Pereira (2022)

13.5 RELATIONSHIP BETWEEN PULLOUT AND SHEAR DISPLACEMENTS

Figures 13.5.1(a) and **13.5.1(b)** show a zero-shear displacement and a large shear displacement condition, respectively, of a shear band intersecting with a reinforcement layer. **Fig. 13.5.1(b)** shows that the pullout displacement of reinforcement at the base of slice No. i (δ_i) is identical to the shear displacement of the base of slice No. *i* (Δ_i):

$$\delta_i = \Delta_i \qquad (13-5-1)$$

The increment of reinforcement pull-out displacement (δ_{incr}) is the difference between the post-loading pullout displacement (δ_b) and pre-loading pullout displacement (δ_a), expressed as:

$$\delta_{incr} = \delta_b - \delta_a \qquad (13-5-2)$$

Corresponding to the incremental pull-out displacement, an incremental pull-out force (T_{incr}) is expressed as:

$$T_{incr} = T_b - T_a \qquad (13-5-3)$$

Where T_a and T_b are pull-out forces mobilized at the pre-loading and post-loading conditions, respectively.

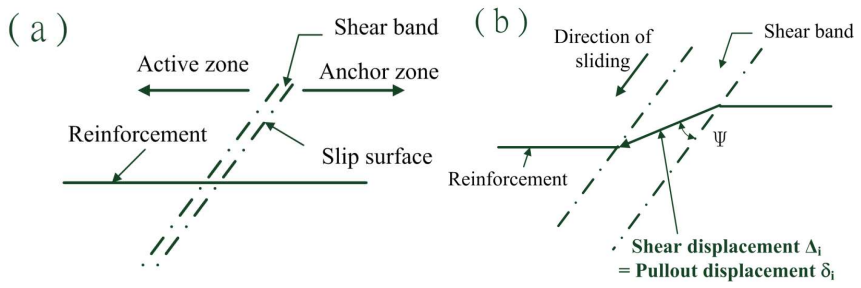

Fig. 13.5.1 Pullout displacement of reinforcement intersecting with a shear band. (a) zero shear displacement condition, (b) large shear displacement condition.

REFERENCES

Cardile, G., Moraci, N. and Calvarano, L.S. (2016) “Geogrid pullout behaviour according to the experimental evaluation of the active length” Geosynthetics International, Vol. 23, No.3, 194-205.

Ferreira, F. B., Vieira, C. S. and Lopes, M. L. (2020) “Pullout behavior of different geosynthetics- Influence of soil density and moisture content” Frontiers in Built Environment, Vol. 6, No. 12, 1-13. Doi: 10.3389/fbuil.2020.00012

Huang, C.-C. (2013) “Force equilibrium-based finite displacement analyses for reinforced slopes: Formulation and verification” Geotextiles and Geomembranes, Vol. 42, pp. 394-404.

Ismail, M.K.A., Joohari, M.I., Habulat, A. and Azizan, F.A. (2021) “Pull-out resistance of sand-geosynthetics reinforcement” The International Journal of Integrated Engineering, Vol. 13, No.3, 87-93. Doi: doi/org/10.30880/ijie.2021.13.03.010

Moraci, N., Cardile, G., Gioffre, D., Mandaglio, M. C., Calvarano, L.S., Carbone, L. (2014) “Soil geosynthetic interaction: Design parameters from experimental and theoretical analysis” Transport Infrastructure and Geotechnical Engineering, Vol. 1, 165-227. Doi: 10.1007/s40515-014-0007-2

Park, J. and Hong, G. (2021) “Effective length prediction and pullout design of geosynthetic strips based on pullout resistance” Materials, Vol. 14, 6151.

Sieira, A.C.C.F., Geoscovich, D.M.S, Sayao, A.S.F.J. (2009) “Displacement and load transfer mechanisms of geogrids under pullout condition” Geotextiles and Geomembranes, Vol. 27, 241-253.

Sugimoto, M. and Alagiyawanna, A.M.N. (2003) “Pullout behavior of geogrid by test and numerical analysis” Journal of geotechnical and geoenvironmental engineering, ASCE, Vol. 129, No. 4, 361-371. Doi: 10.1061/(ASCE)1090-0241(2003)129:4(361)

Tajabadipour, M. and Lajevardi, S.H. (2021) “Laboratory large-scale pullout investigation of a new reinforcement of composite geosynthetic strip” Journal of Rock Mechanics and Geotechnical Engineering, Vol. 13, 1147-1159.

Vieira, C. and Pereira, P.M. (2022) “Influence of the geosynthetic type and compaction conditions on the pullout behaviour of geosynthetics embedded in recycled construction and demolition materials” Sustainability, Vol. 14, 12070. Doi: doi.org/10.3390/su14031207